Biosensors and Bioelectronics 203 (2022) 114046

Contents lists available at ScienceDirect

Biosensors and Bioelectronics

journal homepage: www.elsevier.com/locate/bios

Novel diagnostic and prognostic factors for the advanced melanoma based on the glycosylation-related changes studied by biophysical profiling methods

Anna Sobiepanek [a,*], Patrycja D. Kowalska [a,b], Magdalena Szota [c], Tomasz M. Grzywa [d,e,f], Jakub Nowak [g], Paweł K. Włodarski [d], Ryszard Galus [h], Barbara Jachimska [c], Tomasz Kobiela [a,**]

[a] Faculty of Chemistry, Warsaw University of Technology, Warsaw, Poland
[b] Polish Stem Cell Bank, Warsaw, Poland
[c] Jerzy Haber Institute of Catalysis and Surface Chemistry Polish Academy of Sciences, Krakow, Poland
[d] Department of Methodology, Centre for Preclinical Research, Medical University of Warsaw, Poland
[e] Department of Immunology, Medical University of Warsaw, Warsaw, Poland
[f] Doctoral School, Medical University of Warsaw, Warsaw, Poland
[g] Department of Physical Biochemistry, Faculty of Biochemistry, Biophysics and Biotechnology, Jagiellonian University, Krakow, Poland
[h] Department of Histology and Embryology, Medical University of Warsaw, Warsaw, Poland

ARTICLE INFO

Keywords:
Melanoma
Theranostics
Quartz crystal microbalance with dissipation monitoring
Surface plasmon resonance
Microscale thermophoresis
Lectin-carbohydrate interaction

ABSTRACT

Melanoma is a life-threatening disease due to the early onset of metastasis and frequent resistance to the applied treatment. For now, no single histological, immunohistochemical or serological biomarker was able to provide a precise predictive value for the aggressive behavior in melanoma patients. Thus, the search for quantifying methods allowing a simultaneous diagnosis and prognosis of melanoma patients is highly desirable. By investigating specific molecular interactions with some biosensor-based techniques, one can determine novel prognostic factors for this tumor. In our previous study, we have shown the possibility of a qualitative *in vitro* distinguishing the commercially available melanoma cells at different progression stages based on the measurements of the lectin Concanavalin A interacting with surface glycans present on cells.

Here, we present the results of the quantitative diagnostic and prognostic study of both commercial and patient-derived melanoma cells based on the evaluation of two novel factors: lectin affinity and glycan viscoelastic index obtained from the quartz crystal microbalance with dissipation monitoring (QCM-D) measurements. Two approaches to the QCM-D measurements were applied, the first uses the ability of melanoma cells to grow as a monolayer of cells on the sensor (cell-based sensors), and the second shortens the time of the analysis (suspension cell based-sensors). The results were confirmed by the complementary label-free (atomic force microscopy, AFM; and surface plasmon resonance, SPR) and labeling (lectin-ELISA; and microscale thermophoresis, MST) techniques. This new approach provides additional quantitative diagnosis and a personalized prognosis which can be done simultaneously to the traditional histopathological analysis.

1. Introduction

Cutaneous melanoma remains a threat to global health with increased incidence and mortality rates, in 2020, the number of cases per year was 324,635 and 57,043, respectively (Sung et al., 2021). Melanoma skin cancer develops from melanocytes, cells responsible for producing the photoprotective pigment - melanin (Marczyńska and Przybyło, 2013). Several risk factors for melanoma were identified mainly as excessive exposure to ultraviolet radiation, skin phenotypes I-III, the melanocytic nevi's presence and the patient's specific medical history (Mayer et al., 2014; Gajda and Kaminska-Winciorek, 2014). Melanoma aggressive nature and poor prognostic characteristics are due to its ability to metastasize to various locations. In the early growth phase patients have higher capabilities of survival. However, excision of

* Corresponding author.
** Corresponding author.
E-mail addresses: asobiepanek@ch.pw.edu.pl (A. Sobiepanek), kobiela@ch.pw.edu.pl (T. Kobiela).

https://doi.org/10.1016/j.bios.2022.114046
Received 26 October 2021; Received in revised form 21 January 2022; Accepted 25 January 2022
Available online 29 January 2022

the primary tumor might not prevent metastases in different organs (Elder, 2016). Effective therapy has not been developed yet, due to the low susceptibility of melanoma to standard cancer treatment methods, like radio- and chemotherapy, and the emergence of resistance to targeted therapies.

Thus identifying patients at high risk of metastases development seems crucial (Davey et al., 2016; Sobiepanek et al., 2020b). The standard melanoma diagnostics relies on the observation of dermatoscopic patterns (ABCDE criteria, ugly duckling, or the Glasgow 7-point checklist; Mayer et al., 2014; Gajda and Kaminska-Winciorek, 2014), histopathological assessment (IHC staining of S100 protein, gp100, cytoplasmic protein Melan-A, transcription factors like SOX10 and MITF-1; Prieto and Shea, 2016) or genetic pattern diagnostics (detection of *BRAF, NRAS*, *CDKN2A* and *EPHA3* mutations; Elder, 2016). The qualification of some prognostic factors is essential for deciding about the goals and the treatment method. Various approaches were taken to evaluate the prognosis of patients with cutaneous melanoma. The previous studies have identified demographic and clinical factors, which may affect melanoma patient prognosis. However, the sex, age group, localization and histological type were not statistically significant in melanoma survival (Lideikaitė et al., 2017). On the other hand, the prediction of the disease-free and overall survival based on the Breslow thickness-to-diameter ratio (BDR) is a useful complementary diagnostic tool in cutaneous melanoma assessment; and a cut-off point of 0.15 could be its prognostic limit (Piñero-Madrona et al., 2019). It was proven that no single histological, immunohistochemical or serological biomarker was able to provide a precise predictive value for the aggressive behavior in melanoma patients, regardless of the clinical stage or tumor size; even though the investigated by the IHC staining biomarkers (*e.g.*, HMB-45, PCNA, Ki-67, MMP-2, CD44 and nm23) are well-known to be important in the diagnosis of melanoma (Kycler et al., 2006). Recently, a commercial 31-genetic expression profile (31-GEP) test (DecisionDx-Melanoma, Castle Biosciences Inc, USA) has been validated to predict the risk of metastatic melanoma for patients classified as either class 1 (low risk) or class 2 (high risk). Furthermore, the AJCC Individualized Melanoma Outcome Prediction Tool is often used by clinicians to estimate survival rate and appropriate management recommendations (Farberg et al., 2017). In general, to establish a satisfactory approach for the prognostic analysis, the investigation of melanoma survival should be performed through years on numerous patient group sizes. If necessary, it could also be limited to investigations for one-, five- or ten-year survival (Lideikaitė et al., 2017).

It is necessary to establish new diagnostic methods to confirm the presence of biomarker characteristics for melanoma and assign the malignancy potential of cells in the collected excision. The advanced nanotechnological methods, which bring crucial biophysical information describing normal and cancerous cells/tissues, may be the solution (Sobiepanek and Kobiela, 2018). The distinction between those cells with the measured parameter can be useful as an additional diagnostic procedure. For example, the quartz crystal microbalance (QCM) uses changes in resonant frequency to observe the mass shifts on the sensor (Wang et al., 2012), while the surface plasmons resonance (SPR) utilizes changes in the refractive index of thin metal layers (like gold surfaces) to quantify the binding process of the biomolecule to the sensor surface (Komorek et al., 2021). The atomic force microscopy (AFM) in the spectroscopy mode allows to measure the forces between the probe (functionalized or bare tip) and the sample as a function of their mutual separation. By this method, the determination of cell elasticity and quantification of the ligand-analyte interaction is possible (Lekka et al., 2012; Sobiepanek et al., 2017; Herman et al., 2021). The main advantage of these label-free methods is the possibility of using native biomolecules. At the same time, they permit to quantify the molecular interaction occurring between the molecules by means of the kinetic and/or thermodynamic analysis, as well as viscoelastic properties in the case of investigations performed on the quartz crystal microbalance with dissipation monitoring (QCM-D). A study carried out on cells/tissues as models avoids the long and complicated sample preparations, which may also influence the results (Sobiepanek and Kobiela, 2018, 2022).

During tumor progression, melanoma cells undergo the epithelial-to-mesenchymal-like transformation. This process is connected with the cadherin-switch, the glycosylated proteins localized on the cell membrane. The structural diversity of glycans determines their function in cell proliferation, differentiation, adhesion, cell-to-cell contact and migration (Lityńska et al., 2001; Janik et al., 2016). For years the abnormal glycosylation of peptides, proteins and membrane lipids has been observed in various diseases, including cancer (Przybyło et al., 2002; Hoja-Łukowicz et al., 2017). Glycosylation is defined as the basic difference in cells that undergo cancer transformation. Tumorigenesis and metastasis are frequently associated not only with the altered structure of oligosaccharides in glycoconjugates present on the surface of the cells, but also in the changes in their expression. Intense research has already been performed on the subject with the use of the MALDI-MS analysis (Pocheć et al., 2003; Ciołczyk-Wierzbicka et al., 2004), Western blot analysis (Laidler et al., 2000; Ochwat et al., 2004) as well as RT-qPCR analysis (Laidler et al., 2006) after oligosaccharide, protein or RNA isolation from the cells. Yet, none of the applied methods allow a prognostic model for melanoma or other cancers. Further studies in this topic utilizing whole cells as native samples may be more informative and facilitate diagnosis and prognosis of tumors, as well as the development of targeted therapies. Detection of sugar residuals present in the structure of glycans can be performed with specific lectins as molecular probes (Senkara-Barwijuk et al., 2012; Sobiepanek et al., 2021). Although, QCM technology has been used to investigate lectin-glycan interaction on various cancer cell lines, we are the first group to have applied these QCM-D measurements to the melanoma cell distinguishment (the comparison of the experimental set up and results can be found in Supplementary Materials). Our approach focused on the glycosylation patterns of cells with melanocytic origin combined with biophysical methods can be used to identify potential markers of malignancy, establish novel diagnostic procedures and develop treatment strategies.

In this study, we have used the QCM-D technique with lectin Concanavalin A (Con A) to evaluate quantitatively two prognostic factors for melanoma skin cancer with two approaches: by culturing cells on the sensor's surface before the measurement (cell-based sensors) or by attaching suspension of cells to the sensor surface during the measurement (suspension-cell based sensors). As the first melanoma prognostic factor, we qualified lectin affinity (K_D) towards glycans present on the cell surface. The second one is the viscoelastic index (*VI*), which shows the changes in the glycan viscoelastic properties. The efficiency of these results was further evaluated with complementary methods (including label-free and labeling techniques). To our knowledge, this is the first research paper that shows the relative comparison of the results for the ligand-receptor type measurements performed with the use of whole cells on the microscale thermophoresis (MST) instrument. The analysis of the viscoelastic properties of cells makes it possible to classify them (including patient biopsy) to the type with low or high metastatic potential, regardless of the experience or subjectivity of the operator.

2. Materials and methods

2.1. Cells

The commercial (ATCC) melanoma cell lines used for this study were: WM35 (primary radial growth phase (RGP), CRL-2807), WM115 (primary vertical growth phase (VGP), CRL-1675), WM266-4 (the lymph node metastasis, CRL-1676), MeWo (the lymph node metastasis, HTB-65), G-361 (the solid tumor metastasis, CRL-1424) and A375-P (amelanotic metastasis, CRL-3224). Normal melanocytes HEMa-LP (PCS-200-013, ATCC) were used for comparison. Finally, melanoma cells (MM1, MM7, MM9 and MM16) were isolated from the lymph nodes from a patient of the Maria Skłodowska-Curie Institute of Oncology with

confirmed metastasis (total time needed = 2 weeks). Three methods confirmed the origin and purity of the isolated melanoma cells: cell immunostaining, gene expression and flow cytometry before they were used in this study. A full description of the isolation and characterization of these patient-derived melanoma cell lines (MM1-MM16) is available in Ścieżyńska et al. (2021).

All cells were cultured in RPMI-1640 medium (VWR) containing L-glutamine and supplemented with 10% FBS (Life Technologies), as well as 1% of a penicillin–streptomycin mixture (Life Technologies) in 25 cm^2 culture flasks at 37 °C in the atmosphere of 95% air/5% CO_2. Cells were detached from the flasks using a 0.05% trypsin–EDTA solution (Life Technologies) and seeded on various types of surfaces depending on the measurement type (QCM-D, SPR, lectin-ELISA, AFM, MST). Measurements were performed after culturing cells for 48 h.

2.2. QCM-D lectin-glycan measurements with cell-based sensors

The cell-based experiments were performed using a quartz crystal microbalance working with the dissipation monitoring mode (QCM-D, Q-Sense E1, Biolin Scientific). For these measurements, cells were seeded on the gold sensors coated with polystyrene (Au-PS, QSX 305, Biolin Scientific) placed in a 24-well plate at the density of 5×10^4 cells/well (full procedure described in Sobiepanek and Kobiela, 2022). All measurements were carried out on paraformaldehyde-fixed cells, in the PBST buffer (PBS/0.025% Tween 20, Sigma Aldrich) at 37 °C and with the flow rate set to 25 μl/min, with Con A ranging from 1.6 to 16.0 μM. Each measurement consisted of three steps: washing with PBST (~15 min), lectin-glycan binding (30 min) and washing (30 min), and was performed in triplicate.

The kinetic parameters of the association (k_{on}) and dissociation (k_{off}) rate constants, as well as the dissociation (K_D) constant, were determined using a simple ligand-receptor model as described earlier (Sobiepanek et al., 2017). Furthermore, the lectin flow rate was analyzed in detail from the QCM-D sensorgrams during lectin association to glycans. Finally, the viscoelastic index (*VI*) was calculated as a tangent of the slopes' angle obtained on the D(f) plots of each measurement (thanks to simultaneous measurements of changes in both parameters: frequency and dissipation factor; more details can be found in Sobiepanek and Kobiela, 2022).

2.3. Lectin-ELISA assay

Con A binding to the glycans present on the cell surface was measured with a multi-mode microplate reader (Synergy H4, Biotek) with the procedure described in Sobiepanek et al., (2017). Cells were seeded into the 96-well plate at the density of 1×10^4 cells/well, incubated for 48 h at 37 °C, fixed and stained with various concentrations of FITC-conjugated Con A (1.6–12.8 μM in PBST, Sigma Aldrich), Hoechst 33342 dye (1 μg/ml in PBS, Thermofisher). Cells were measured with the excitation 350 nm and emission 461 nm for nuclei staining (Hoechst), as well as ex. 490 nm and em. 525 nm for glycan staining (Con A–FITC). The results are presented in the form of fluorescence intensity (in relative fluorescence units, RFU) dependence as a function of Con A–FITC concentration. Each experiment was performed in triplicate.

2.4. Whole-cell SPR measurements of the lectin-glycan interaction

In the angular scan measurement mode, the lectin-glycan interaction was also analyzed with the multi-parametric surface plasmon resonance (MP-SPR model Navi 200, BioNavis Ltd.). During these measurements, cells were seeded on gold sensors coated with polystyrene (Au-PS, BioNavis Ltd.) placed in a 6-well plate at the density of 2.5×10^5 cells/well, incubated for 48 h and fixed. Measurements were carried out at a 785 nm laser wavelength in the PBST buffer at 37 °C, with the flow rate set to 50 μl/min, and 12.8 μM Con A solution. Each measurement was divided into three steps: washing with PBST (~10 min), lectin-glycan binding (30 min) and washing (30 min), and was performed in triplicate. In addition, the SPR sensorgram presents the time-dependent changes in the resonance angle (ΔΘ) and the differences in the lectin flow rates during its binding with glycans were also calculated. Data was analyzed with the MP-SPR Navi™ data viewer and Sigma Plot software.

2.5. Elasticity measurements of melanoma cells

The elasticity of cells was measured using a commercial atomic force microscope (XE120 model, Park Scientific Instruments) and an optical microscope to control the position of the gold-coated silicon nitride cantilevers (MLCT-C, Bruker) with a nominal spring constant of 0.01 N/m. Cells were seeded on glass coverslips (Marienfeld, 10 mm diameter) placed in 24-well plates at the density of 2×10^4 cells/well for 48 h incubation. All AFM measurements were performed at room temperature in the RPMI-1640 medium without FBS.

Force curves were collected randomly from chosen cells from the region around the cell center. The force was set up to 4 nN, the approach velocity to 9 μm/s and a grid of 4 × 4 points on each cell was selected. The E values were calculated based on the subtraction of the two force curves: the calibration curve recorded on the glass coverslip without the cells and the other curves collected on a given cell (Kobiela et al., 2013). The obtained *force-versus-indentation-curve* was analyzed by means of the Sneddon extension of the Hertz model, assuming that the tip is an infinitely stiff indenter modeled by a parabola (full description available in Sobiepanek et al., 2016). The results are presented for the indentation depth of 300 nm. Each experiment was performed in triplicate.

2.6. QCM-D lectin-glycan measurements with the suspension cell-based sensors

Experiments with the suspension cell based-sensors were prepared in the following steps: 1 – clean gold sensor (QSX 301, Biolin Scientific) coating with 0.01% poly-L-lysine solution (PLL, Sigma Aldrich) for 5 min at room temperature; 2 – mechanical detachment of cells from the 6-well plate, cell centrifugation (581×*g*) and resuspension in PBST to the density of 1×10^6 cells/ml; 3 – QCM-D measurements of cell binding to Au-PLL sensor (30 min, 37 °C, 25 μl/min); 4 – QCM-D measurements of the lectin binding to the freshly attached cells (full procedure described in Sobiepanek and Kobiela, 2022). These measurements were also carried out at 37 °C and with the flow rate set to 25 μl/min, with the Con A ranging from 0.8 to 3.2 μM. Each experiment was performed in triplicate. Analysis of the lectin-glycan binding was performed analogically like in subsection 2.2.

2.7. Whole-cell MST measurements of the lectin-glycan interaction

For the microscale thermophoresis (MST) measurements performed on Monolith.115 instrument (NanoTemper Technologies), cells were mechanically detached from the 6-well plate, centrifuged at 581×*g*, resuspended in PBST and diluted to the density of 5×10^4 cells in 10 μl in the first sample. In total, 16 dilutions were prepared according to the geometric dilution quotient of 0.5. Next, 10 μl of the lectin Con A-FITC solution (100 nM in PBST) was added to each sample with cells in proportion 1:1 (final concentration of 50 nM lectin in all samples). The samples were loaded into the capillaries Premium MST (NanoTemper Technologies) and inserted into the apparatus with the temperature set at 37 °C. The laser intensity was set to 40% LED power and low MST power. Data were analyzed with MO.Affinity Analysis software (NanoTemper Technologies). The relative comparison of EC_{50}-like parameter (the effective dose of ligand) was estimated based on a simple equilibrium model and the equation ($EC_{50} = K_D + 0.5 \cdot [target\ concentration]$), where it describes concertation at which half of all target molecules are present in the bound state (more information on the applied model may be found in the NanoTemper Technologies materials for users). The

numerical results are presented as a ratio between the obtained EC_{50}-like parameter for the primary and metastatic cells. Each experiment was performed in duplicate.

2.8. Statistical analysis

The statistical analysis was performed using a single-factor ANOVA with the Student's post hoc *t*-test. The statistical significance was marked on each graph, where the p-value was below 0.05 (*) or 0.1 (#). The mean values were determined from three independent experiments.

3. Results and discussion

3.1. Evaluation of the methodology for melanoma prognostic factors with commercial cell lines

We have used lectin Concanavalin A to quantify its interaction with mannose and glucose residuals present on cells using the QCM-D method. Different melanocyte-originating cells were seeded on polystyrene-coated gold sensors, cultured for 48 h and fixed. This approach is referred to later as the cell-based protocol. Using the sensors on which these fixed cells were attached, the lectin-glycan interaction measurements were performed to obtain the real-time changes in two parameters: frequency and dissipation factor. Changes in frequency are related to the bound mass of the analyte (Con A) to the sensor's surface, which can be further analyzed with various models of interaction. Seven commercial cell lines were measured with various Con A concentrations. The relaxation time was calculated for each lectin concentration using a simple ligand-receptor model from a single measurement. Afterward, the association and dissociation rate constants, which describe the formation of the lectin-glycan complex, were determined by plotting the reverse in relaxation time as a function of Con A concentrations (Mori et al., 2010). Examples of the kinetic analysis results for the two closely related cell lines (commercial cells isolated from the same patient: WM115 – primary VGP melanoma and WM266-4 metastasis to the lymph node) are shown in Fig. 1A. We calculated the dissociation constant from the received linear regressions, whose value for all measured cells is presented in Fig. 1C. The received nanomolar range of the K_D values for these measurements is consistent with literature data for other cell types (Peiris et al., 2012; Li et al., 2013). The normal melanocytes (HEMa-LP) and non-invasive RGP melanoma cells (WM35) were poorly distinguishable by affinity (K_D value at the level of 2.85 nM and 2.49 nM, respectively). The affinity of Con A to glycans was significantly different for the slightly invasive VGP melanoma cells (WM115, $K_D = 0.94$ nM) in comparison with other cells and in the case of all metastatic cells (G-361, MeWo, WM266–4, A375-P) the affinity was very high ($K_D < 0.40$ nM). These data stay in agreement with our previous reports (Sobiepanek et al., 2017) and fall within the affinity range described in the literature for lectin-glycan interactions: 0.362 nM (Con A and breast cancer cells SKBR-3; Peiris et al., 2017) to even 980 μM (HPA and colorectal cancer cells SW620; Peiris et al., 2012) (full literature comparison can be found in Supplementary Materials).

To verify the affinity results of the lectin-glycan interaction, we have used the lectin-ELISA assay. The fluorescence intensity values for Con A-FITC analysis were plotted against the lectin concentration and are presented in Fig. 1B. In the following step, the data was fitted by the linear regression and the obtained results allow us to conclude that with the rising metastatic potential of cells the slope value has increased. Slope values (Fig. 1C) for normal cells and cells from both primary sites (RGP and VGP) are below 900 RFU and for all metastatic cells, these values are above 900 RFU. However, some metastatic cells present significantly higher slope values (WM266–4 and A375-P) than others (MeWo and G-361) without a distinction of the direct site of metastasis (lymph node, solid tumor).

To further understand the mechanism by which the lectin-glycan interaction occurs on the cells, we have used the MP-SPR instrument. It is the most recognized label-free technique for studying the ligand-receptor interaction. Comparing SPR results with the ones obtained from QCM-D makes it possible to determine the water content in the formed layer (Komorek et al., 2020). Two closely related cell lines (primary VGP WM115 and metastatic WM266-4) were used for this analysis on the polystyrene-coated SPR sensors and the interaction results of 12.8 μM lectin Con A with glycans were registered on the SPR sensorgrams (Fig. 2A). Two stages of the lectin adsorption on the glycans can be recognized for both cell lines: rapid stage 1 with a strongly increased signal, and stage 2, which takes some time until the signal stabilization is almost reached. However, the washing step brings the signal back to the value from the first stage, which indicates that this

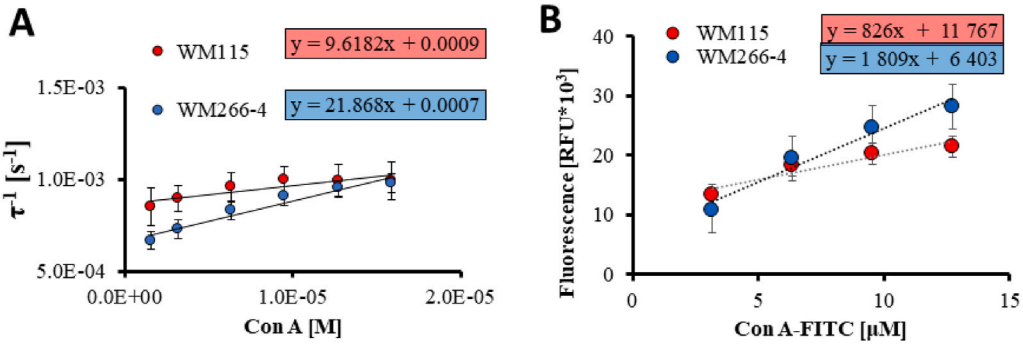

C

Melanocytic cell type	Cell line	QCM-D K_D [nM]	Lectin-ELISA FLUO equation
Normal	HEMa-LP	2.85	y=668x+6372
RGP	WM35	2.49	y=725x+12047
VGP	WM115	0.94	y=826+11767
Lymp node metastasis	WM266-4	0.32	y=1809x+6403
	MeWo	0.35	y=908x+7113
Solid tumor metastasis	A375-P	0.28	y=1641x+9139
	G-361	0.39	y=977x+8002

Fig. 1. Results of the lectin-glycan interaction study on melanocyte-originating cells. A – the corresponding relation of the reverse in relaxation time plotted as a function of Con A concentration for QCM-D measurements performed on the primary VGP melanoma (WM115) and the lymph node metastatic cells (WM266-4). B – lectin-ELISA results of the fluorescent intensity for bound Con A-FITC to WM115 and WM266-4 cells. C – quantitative results obtained from the QCM-D kinetic analysis (affinity, K_D) and the lectin-ELISA analysis (equation) for different commercial cell lines.

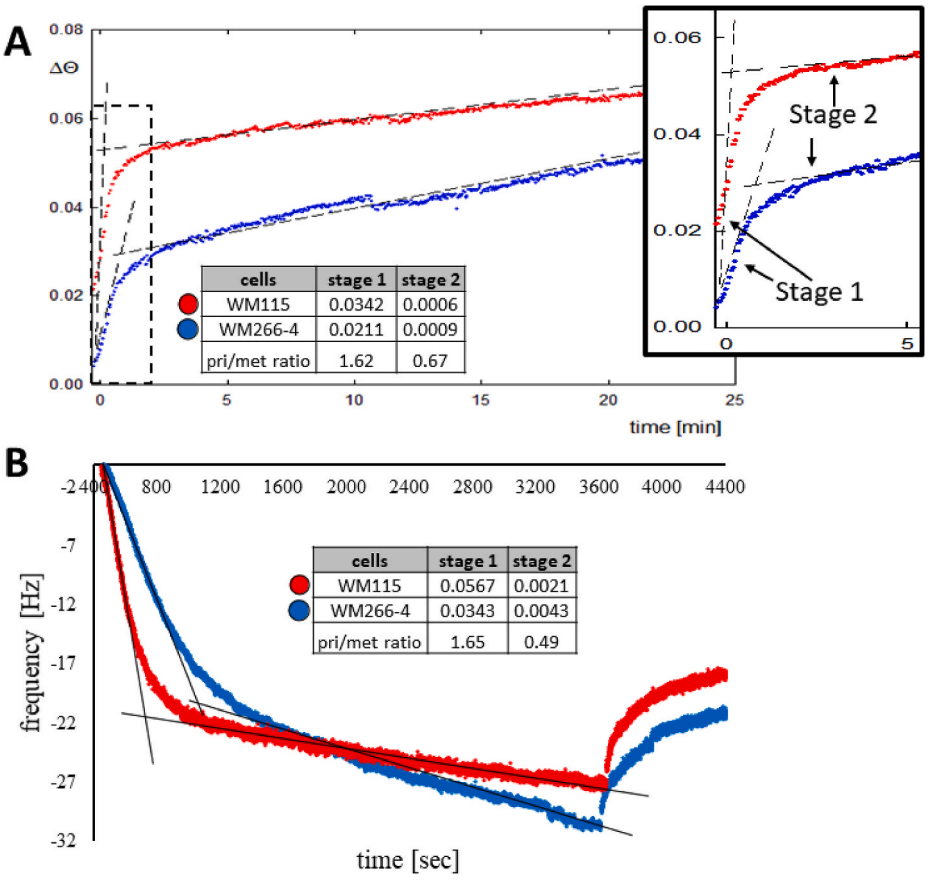

Fig. 2. Results of the cell-based measurements of the lectin-glycan interaction study on the primary VGP melanoma (WM115) and the lymph node metastatic cells (WM266-4) cells. The distinction of the two phases of the lectin flow rate analysis on SPR sensorgram (A) and QCM-D sensorgrams (B) for Con A binding to glycans present on melanoma cells.

stage determines the effectiveness of the lectin-glycan interaction on the cells. The primary melanoma cells are distinguishable from the metastatic ones at both stages based on the slope curve, although the primary/metastatic ratio changes (stage 1 = 1.62, stage 2 = 0.67). This difference in the linear regression for both stages of the association can be explained by the rising concentration of Con A during the experiment, which binds first to the most available sugar residues and next tries to bind to the less available sites of the glycans. As identified earlier, primary melanoma possesses short and less ramified glycans, whereas metastatic melanoma cells long, branched mannose and glucose types of oligosaccharides (Ciołczyk-Wierzbicka et al., 2004). In literature, a higher concentration of Con A increased the monovalent interactions and limited the possibility of its rebinding to another sugar residue (Sandoval-Altamirano et al., 2017). It seems that the increment of the signal may be a characteristic value for a specific cell line at each stage (primary melanoma gives higher signals at stage 1 and metastatic cells at stage 2). Moreover, the two stages of the association can also be found in the QCM-D results after a detailed analysis (Fig. 2B) and the primary/-metastatic ratio changes of the slop curve are comparable (stage 1 = 1.65, stage 2 = 0.49) with the SPR results. Although the changes in frequency on the QCM-D results are significantly higher than the signal on the SPR sensorgrams, this confirms that the hydration in these measurements plays an important role. Obviously, the degree of hydration of the layer has a crucial influence on the protein layer viscoelastic properties (Jachimska and Tokarczyk, 2016; Komorek et al., 2021). Even though SPR gains more attention with the whole-cell studies such as ligand-receptor interactions or compound uptake (Viitala et al., 2013; Yanase et al., 2014; Suutari et al., 2020), this method is not easily applied.

The ability to simultaneously measure changes in frequency and dissipation factor on the QCM-D allows us to obtain more information about the viscoelastic properties of the lectin-glycan complexes (the viscoelastic signatures of the cells). Having in mind, that glycans present on the surface of the cells can be short and lowly-branched, or long and highly-branched depending on the stage of the tumor progression (Ciołczyk-Wierzbicka et. Al. 2004), lectin Con A can be used as a melanoma biomarker by detecting changes in these structures with the QCM-D measurements. Data changes in the dissipation factor (D) versus changes in the frequency (f) were plotted for each cell line. The example of the D(f) plots obtained for VGP and metastatic melanoma cells with Con A concentration of 6.4 μM are present in Fig. 3A. The viscoelastic index (*VI*) parameter can describe differences in the viscoelastic properties of the created lectin-glycan complexes. Its value is equal to the slope of a line tangent to the curve visible on the Df plots (Sobiepanek and Kobiela, 2022). The lower the VI value is, the less elastic complex (short and lowly-branched glycans bound by lectin Con A) is created on the surface of the sensor. Thus, the linear regression was matched for each D(f) relation focusing on the first 10 min of the measurement, which corresponds to the more effective stage 1 of the lectin-glycan interaction on cells as determined *via* the QCM-D/SPR analysis. The obtained VI values enable to order melanoma cell lines according to the increasing curve angle (*i.e.,* cells with increasing tumor potential, Fig. 3D). When analyzing the total range of VI values for these measurements (Fig. 3B), the lowest values were obtained for normal cells (HEMa-LP) and RGP cells (WM35) ($VI_{av} < 0.3$) (average VI values were 0.12 and 0.26, respectively). But with the rising tumorigenic potential of cells, the viscoelastic index increased its value (for VGP melanoma the average VI value was 0.4). Metastatic melanoma cells MeWo and A375-P

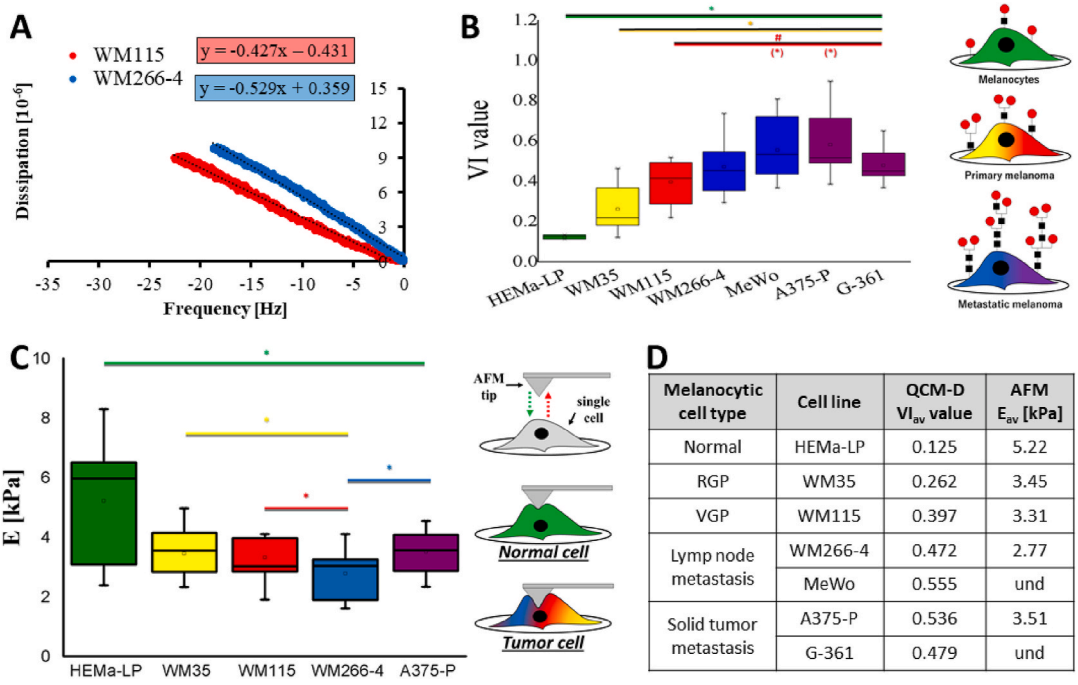

Melanocytic cell type	Cell line	QCM-D VI_{av} value	AFM E_{av} [kPa]
Normal	HEMa-LP	0.125	5.22
RGP	WM35	0.262	3.45
VGP	WM115	0.397	3.31
Lymp node metastasis	WM266-4	0.472	2.77
	MeWo	0.555	und
Solid tumor metastasis	A375-P	0.536	3.51
	G-361	0.479	und

Fig. 3. Results of the viscoelastic analysis. A – example Df plots for the 7th overtone of the QCM-D interaction measurements performed on the primary WM115 and metastatic WM266-4 melanoma cell lines for the 6.4 μM concentration of Con A. B – an overview of the obtained viscoelastic index values for Con A concentrations (1.6–12.8 μM) interacting with glycans present on cells: melanocytes (HEMa-LP), RGP cells (WM35), VGP cells (WM115), as well as metastatic cells from the lymph node (WM266-4, MeWo) and the solid tumor metastatic site (A375-P, G-361). C – elastic modulus of melanocyte-originating cells obtained by means of AFM measurements with the graphical introduction to methodology. D – quantitative results obtained from the QCM-D viscoelastic analysis (viscoelastic index, VI) and the AFM analysis (elastic modulus, E) for different commercial cell lines.

presented the highest average VI values (>0.5) and for WM266-4 as well as G-361 the VI_{av} value was almost equal to 0.5.

Although a viscoelastic analysis of the QCM-D experiments brings valuable information about the layer present on the sensor, it is not very common in the case of the cell study. The Df plots analysis was typically made for proteins or polymers (*e.g.,* dendrimers) in various conditions deposited on well-defined surfaces (Jachimska and Pajor, 2012; Jachimska et al., 2013). In a cell study, it was mainly used in measurements of their adhesion to modified surfaces of the sensors (Zhou et al., 2012; Kılıç and Kok, 2018) or to check the cytotoxic effect of compounds (cell death - apoptosis/necrosis, morphological/cytoskeletal changes - rounding, shrinkage lysis) (Fatisson et al., 2011; Nowacki et al., 2015; Staniszewska et al., 2020). The achieved QCM-D results show that the flexibility of lectin-glycan complexes (viscoelastic signatures) on cells is due to the co-existence of rigid saccharides and flexible glycosidic linkage units in glycan structure (Re et al., 2012). The obtained differences of VI values for various cells are connected with the changes in the studied glycan structure, which occurs during melanoma development. As MALDI-MS analysis confirmed, metastatic A375-P cells possess long and highly-branched glycans with terminal mannose residues and WM35 cells from the primary RGP site relatively short and lowly-branched glycans with terminal mannose residues (Ciołczyk-Wierzbicka et al., 2004). Nevertheless, this method brings detailed knowledge of the hypothetical structures present on cells, it requires several steps including cell homogenization, electrophoresis and Western blotting, MALDI-MS analysis, and a comparison of the results with the appropriate database. On the other hand, the LC-MS/MS method can also be used to determine the carbohydrate composition, sequence and branching of monosaccharides, inter-glycosidic linkages as well as anomeric connectivity, but it requires a similar process of the sample preparation (Zhou et al., 2017). Our results do not show the exact composition of carbohydrates in glycans, but it enables to observe the flexibility of the lectin-glycan complex (a characteristic viscoelastic signature of each cell type) as well as the affinity of lectin to glycans (Sobiepanek and Kobiela, 2022), which was proved to be sufficient for the quantitative distinction all cell type: normal cells, primary tumor site cells and metastatic cells.

This stays in contrast to the measurements of elastic properties of cells performed with the AFM technique in the force spectroscopy mode, where the biomechanical parameters of the investigated cells permit to distinguish only melanocytes from melanoma cells (Fig. 3C–D). The average value of the elastic modulus was almost two times higher for the HEMa-LP cells ($E = 5.22 \pm 1.89$ kPa). This result stays in line with other literature data, which suggests that cancer cells are generally softer than normal cells - less resistant to deformation (Lekka et al. 1999, 2012; Gostek et al., 2015). Interestingly, the E values for VGP W115 and metastatic WM266-4, which were isolated from the same patient, were significantly different. These results confirm the theory of the more deformable metastatic cells than cells from the primary site. However, one must bear in mind that stiffness is a dynamic property of melanoma cells and the cell ability to vary their degree of elasticity towards both very low and very high values (Weder et al., 2014). Therefore, changes in melanoma cell stiffness cannot be interpreted clearly and the AFM analysis for diagnostic purposes in the case of patients with melanoma should be approached with extreme caution.

Considering the established cell-based model on the commercially available cell lines, the affinity of lectin Con A is much higher to the metastatic melanoma cell lines than to cells from the primary site and normal cells. Furthermore, the viscoelastic properties of the created complexes increased with the rising metastatic potential of the cells. For metastatic melanoma cells both parameters have high values: the affinity of Con A to glycans on cells ($K_D < 0.5$ nM) and the viscoelastic index ($VI > 0.5$). As shown, the established method is universal and can be applied for all kinds of cells irrespective of the occurrence or absence of mutations in genes typical for melanoma (*e.g., BRAF* – not identified in the MeWo cell line).

3.2. Verification of the cell-based method to rate the high/low metastatic potential of patient cells

Four different melanoma cell subtypes were isolated from a lymph node of a patient with confirmed metastasis, and next their purity and origin were confirmed before use in this study within 2 weeks from the biopsy. These cell lines varied in morphology (epithelioid shape of MM1, MM7, MM9 and spindle of MM16), doubling times (32–33 h for MM7 and MM9, 42–43 h for MM1 and MM16) (Ścieżyńska et al., 2021) and even elastic properties (Fig. 4A). These cells can be divided into two groups based on the cell elastic values: cells with medium stiffness (MM1 = 4.7 ± 1.3 kPa, MM16 = 3.0 ± 1.4 kPa and MM9 = 2.3 ± 0.5 kPa) and stiffer cells (MM7 = 6.6 ± 2.9 kPa). These cell populations are heterologous in terms of cell elasticity, which is frequently observed in cancer cells, including commercial melanoma cell lines (Bobrowska et al., 2019). The QCM-D measurements of the lectin affinity to the isolated melanoma cells (Fig. 4B) show that the MM1 cells presented the highest K_D value 2.1 nM (similarly to RGP melanoma cells WM35 = 2.5 nM) and MM16 cells the value of 1.0 nM (almost equal to the K_D value received for VGP cells = 0.9 nM). The remaining 2 subtypes of the isolated cells (MM7 and MM9) were of identical affinity values like for the metastatic cell lines (0.2–0.3 nM). Thus, the received affinity results suggest that especially cells MM7 and MM9 have a high metastatic potential. The results of the lectin-ELISA assay (Fig. 4C), though slightly lower than for commercial cells, show that the slope values for MM7 and MM9 cells are between 500 and 700 RFU and for MM1 and MM16 cells 350–500 RFU. This confirms that a higher metastatic potential is observed in MM7 and MM9 cells. When analyzing the viscoelastic index of the isolated cells (Fig. 4D–F), the average values enable to distinguish cells with a rising tumorigenic potential. MM1 and MM16 cells present the VI value comparable to melanocytes and RGP melanoma (VI_{av} < 0.3). The VI values are also comparable for MM7, MM9 cells and VGP melanoma (VI_{av}~0.3), which have a slight invasive potential. With respect to these results, MM1 and MM16 cells may be treated as cells with a lower metastatic potential, and MM7 as well as MM9 as cells with a rising metastatic potential. The presented results confirm that the isolated melanoma cells have different glycosylation profiles measured by the cell-based QCM-D protocol. The described prognostic factors of lectin affinity and viscoelastic index allowed us to assess the metastatic potential of these cells much more accurately and quantitatively than the traditional diagnostic procedures.

3.3. The usability of the suspension cell-based sensors to receive reliable melanoma prognostic factors

The QCM-D cell-based procedure described above is carried out for at least 3 days (1- cell seeding, 2- potential time for the drug addition, 3- measurements and result analysis), which is quite long. If this procedure were to be included as a standard diagnostic test, it should be shortened. For this aid, we have further modified the procedure to enable a faster distinction of the cells by using a suspension of cells directly in the measurements and eliminating the cell seeding part on the sensors (1-day procedure = measurement and analysis of the result, Fig. 5A). Cells were transferred into suspension by a gentle mechanical detachment and their concentration was evaluated to use the same number of cells for each experiment. The first part of the QCM-D experiment required binding the cells from the suspension to the surface of the sensor. This was realized by modifying a gold sensor with a poly-L-lysine solution, a positively charged polymer facilitating cell adhesion through the attraction of their negatively charged membrane (Sobiepanek et al., 2020a). Cells were introduced into the chamber and the cell binding to the surface was measured through QCM-D. The attached cells were washed with a PBST buffer solution, and the lectin Con A was inserted into the chamber for the lectin-glycan interaction measurement. As investigated by Wang et al. (2012), the concentration of lectin had to be reduced due to the PLL-coating of the sensor and higher probability of the non-specific binding. Thus, the Con A concentration applied for the lectin-glycan interaction was in the range of 0.8–3.2 μM. The kinetic and

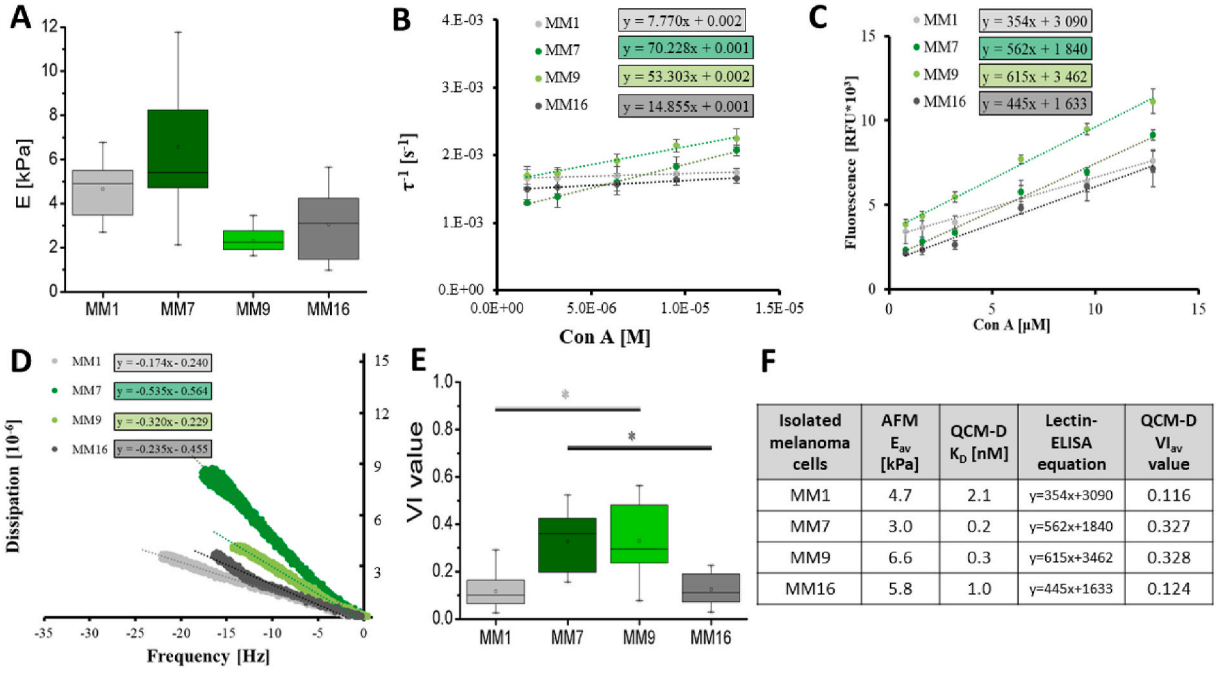

Isolated melanoma cells	AFM E_{av} [kPa]	QCM-D K_D [nM]	Lectin-ELISA equation	QCM-D VI_{av} value
MM1	4.7	2.1	y=354x+3090	0.116
MM7	3.0	0.2	y=562x+1840	0.327
MM9	6.6	0.3	y=615x+3462	0.328
MM16	5.8	1.0	y=445x+1633	0.124

Fig. 4. Results obtained with the isolated melanoma cells. A – elastic modulus of cells obtained by means of AFM measurements. B – the corresponding relation of the reverse in relaxation time plotted as a function of Con A concentration for QCM-D measurements. C – lectin-ELISA results of the fluorescent intensity for bound Con A-FITC to the cells. D – the example of Df plots for the 7th overtone of the QCM-D interaction measurements performed on the isolated melanoma cells for the 6.4 μM concentration of Con A. E – an overview of the obtained viscoelastic index values for Con A concentrations (1.6–12.8 μM) interacting with glycans present on isolated melanoma cells. F – quantitative results recieved from the AFM analysis (elastic modulus, E), the QCM-D kinetic analysis (affinity, K_D), the lectin-ELISA analysis (equation) and the QCM-D viscoelastic analysis (viscoelastic index, VI).

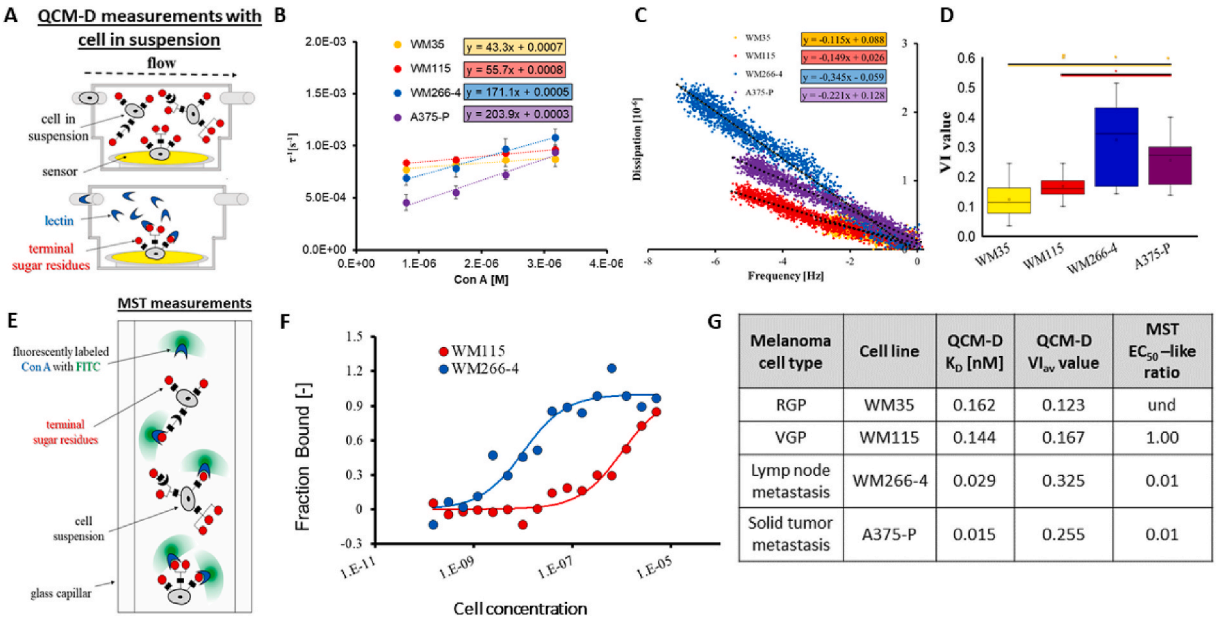

G

Melanoma cell type	Cell line	QCM-D K_D [nM]	QCM-D VI_{av} value	MST EC_{50}–like ratio
RGP	WM35	0.162	0.123	und
VGP	WM115	0.144	0.167	1.00
Lymp node metastasis	WM266-4	0.029	0.325	0.01
Solid tumor metastasis	A375-P	0.015	0.255	0.01

Fig. 5. Results obtained with the melanoma cells in suspension. A – the graphical introduction to the QCM-D with cell suspension methodology. B – the corresponding relation of the reverse in relaxation time plotted as a function of Con A concentration for suspension cell-based sensors. C – the example of Df plots for the 7th overtone of the QCM-D interaction measurements performed on the freshly adhered cells from suspension for the 1.6 μM concentration of Con A. D – an overview of the obtained viscoelastic index values for Con A concentrations (0.8–3.2 μM) interacting with glycans present on isolated melanoma cells. E – the graphical introduction to the MST with cell suspension methodology. F – the MST results of the lectin-glycan binding curve for WM115 and WM266-4 cell lines. G – quantitative results recieved from the QCM-D kinetic analysis (affinity, K_D), the QCM-D viscoelastic analysis (viscoelastic index, VI) and the MST binding analysis (EC_{50}-like).

viscoelastic analysis results are presented in Fig. 5B and C, respectively. The association rate constants differ significantly for the primary melanoma sites (RGP and VGP) and metastatic melanoma cells, which translates into the lectin affinity values presented in Fig. 5G. The K_D values are 5- to 10-times different depending on the analyzed cell lines. This means that it is easier to distinguish cells based on the kinetic analysis of the lectin-glycan interaction with the suspension cell-based sensors than in the cell-based procedure (K_D value was only 2- to 3-times different). The viscoelastic analysis of the created complexes (Fig. 5C–D) shows that the primary RGP site (WM35) and VGP site (WM115) were of much lower VI values ($VI_{av} < 0.2$) than the VI values for the metastatic cells ($VI_{av} > 0.25$), allowing for a clear distinction between melanoma progression phases. With this analysis, one must bear in mind that the VI values strongly depend on the lectin concentration and must be lower than in the case of the cell-based procedure. To our knowledge, this was the first attempt to perform the ligand-receptor QCM-D analysis on adherent cells which were transferred to suspension for measurement.

The specific form of the cells in these measurements limits the number of methods used to compare and evaluate the lectin-glycan interaction. Microscale thermophoresis is a labeling technique, which permits to follow the interaction of molecules in suspension in real-time. Typical biomolecular interactions measured by means of MST range from protein–DNA, protein–protein, protein–small molecule and protein–liposome interactions, where the concentrations of each molecule are well-known (Jerabek-Willemsen et al., 2014). However, in our case, the direct value of the affinity was not possible to calculate due to the unknown concentration of glycans on the surface of the cell. Thus, the relative comparison of the effective dose of ligand was estimated based on a simple equilibrium model and the equation to receive the parameter EC_{50}-like at which half of all target molecules are present in the bound state. The results of lectin Con A-FITC interacting with glycans present on the whole cells in suspension are gathered in Fig. 5F and the resulting ratio of EC_{50}-like values in Fig. 5G. The primary VGP cells exhibited significantly lower EC_{50} values than all metastatic cells (100-times different). This is one of the first approaches to the whole-cell study by means of MST techniques, as most of the described analysis utilizes cell lysates for their known molar concentration (Magnez et al., 2017). The other noted attempt is the measurement of the interaction between labeled anti-CD42b antibody and CD42b receptor expressed on the surface of human platelets (Lindahl and Macwan, NanoTemper application note).

4. Conclusions

The analysis of biomolecular interactions has become essential for developing innovative, more efficient techniques for the diagnosis and prognosis of various cancers. Currently, because there are no single histological, immunohistochemical or serological biomarkers recognized for predicting melanoma aggressive behavior and the prognosis for melanoma patients is poor due to the frequent development of resistance to drugs, advanced research conducted for this tumor is essential. Thus, the presented study aimed to establish a quantitative distinguishment of cells from different progression stages of melanoma based on the glycosylation profile of cells. Both established procedures of the lectin-glycan interaction performed on cell-based sensors and the suspension cell-based sensors show the possibility of differentiating cells from the following stages of melanoma progression. This was achieved by characterizing two prognostic factors from the QCM-D lectin-glycan measurements: the affinity and viscoelastic index. Lectin Con A has a much higher affinity towards metastatic melanoma cells, where the affinity for the primary melanoma and melanocytes is lower. On the other hand, the viscoelastic index obtained from the lectin-glycan measurements shows that the value significantly rises with the increasing cell potential for metastasis. These results were confirmed by complementary biophysical methods: AFM, SPR and MST. It is worth mentioning that this is the first research paper showing the relative comparison of the results for the ligand-receptor type measurements performed with the use of whole cells on the MST instrument. Our methodology was successfully applied not only on the commercially available human cell

lines, but also verified with cells isolated from a patient with confirmed melanoma metastasis (in 2 weeks) validating its usability to distinguish the metastatic potential of cells. Especially important for the patient's health are the results obtained with the suspension cell-based sensors; where the duration of the procedure was significantly shortened (from 3 to 1 day) compared to the cell-based sensors with a simultaneous increase in sensitivity (10-times different affinity values). Considering our results, the proposed model can be a milestone to personalized diagnosis, prognosis and therapy monitoring.

Author contribution

AS and TK designed the study and performed the literature search. AS, PDK, MS and TMG performed the experiments. AS, JN, PW, RG, BJ and TK analyzed the data. AS wrote the original draft of the manuscript. AS, BJ and TK reviewed and edited the manuscript. All authors have read and agreed on the final version of the manuscript.

Ethical statement

This study was approved by the local Ethics Committees at the Medical University of Warsaw no. KB/216/2017. Written informed consent was obtained from the patient.

Declaration of competing interest

The authors declare that they have no known competing financial interests or personal relationships that could have appeared to influence the work reported in this paper.

Acknowledgments

This work was financially supported by the National Science Center (Poland) PRELUDIUM 14 project no. 2017/27/N/ST4/01389, and BIOTECHMED-1 project granted by the Warsaw University of Technology under the program Excellence Initiative: Research University (ID-UB). Additionally, AS would like to express her thanks for the doctoral scholarship NCN ETIUDA 6 (no. 2018/28/T/ST4/00511). The authors are grateful to Prof. Małgorzata Lekka (Institute of Nuclear Physics PAS) for the cell lines (HEMa-LP, WM35, WM115 and WM266–4, A375-P), to Dr. Marcin Zdzienicki (Maria Skłodowska-Curie Institute of Oncology, Warsaw) for providing the biopsies with metastatic melanoma, to Dr. Maria Stepaniuk (Children's Memorial Health Institute) for performing the IHC staining of the isolated melanoma cells and to Paulina Kośka (MSc. Eng. student) for her assistance in the QCM-D measurements with the suspension cell based-sensors. The authors are also obliged to Prof. Jan Antosiewicz (University of Warsaw) for fruitful discussions. This work was performed at the Warsaw University of Technology, the Medical University of Warsaw, and the Institute of Catalysis and Surface Chemistry PAS. The Monolith system was made available for this research free of charge by NanoTemper Technologies thanks to Dr. Natalia Kubisa.

Appendix A. Supplementary data

Supplementary data to this article can be found online at https://doi.org/10.1016/j.bios.2022.114046.

References

Bobrowska, J., Awsiuk, K., Pabijan, J., Bobrowski, P., Lekki, J., Sowa, K.M., Rysz, J., Budkowski, A., Lekka, M., 2019. Anal. Chem. 91, 9885–9892. https://doi.org/10.1021/acs.analchem.9b01542.

Ciołczyk-Wierzbicka, D., Amoresano, A., Casbarra, A., Hoja-Łukowicz, D., Lityńska, A., Laidler, P., 2004. Glycoconj. J. 20, 483–492. https://doi.org/10.1023/B:GLYC.0000038294.72088.b0.

Davey, R.J., van der Westhuizen, A., Bowden, N.A., 2016. Crit. Rev. Oncol. Hematol. 98, 242–253. https://doi.org/10.1016/j.critrevonc.2015.11.011.

Elder, D.E., 2016. Pathology 48, 147–154. https://doi.org/10.1016/j.pathol.2015.12.002.

Farberg, A.S., Glazer, A.M., Winkelmann, R.R., Rigel, D.S., 2017. Dermatol. Clin. 35, 545–550. https://doi.org/10.1016/j.det.2017.06.017.

Fatisson, J., Azari, F., Tufenkji, N., 2011. Biosens. Bioelectron. 26, 3207–3212. https://doi.org/10.1016/j.bios.2010.12.027.

Gajda, M., Kaminska-Winciorek, G., 2014. Asian Pac. J. Cancer Prev. APJCP 15, 3873–3877. https://doi.org/10.7314/APJCP.2014.15.9.3873.

Gostek, J., Prauzner-Bechcicki, S., Nimmervoll, B., Mayr, K., Pabijan, J., Hinterdorfer, P., Chtcheglova, L.A., Lekka, M., 2015. Eur. Biophys. J. 44, 49–55. https://doi.org/10.1007/s00249-014-1000-y.

Herman, K., Zemła, J., Ptak, A., Lekka, M., 2021. Phys. Rev. E 104, 024409. https://doi.org/10.1103/PhysRevE.104.024409.

Hoja-Łukowicz, D., Przybyło, M., Duda, M., Pocheć, E., Bubka, M., 2017. Biochim. Biophys. Acta Gen. Subj. 1861, 3237–3257. https://doi.org/10.1016/j.bbagen.2016.08.007.

Jachimska, B., Łapczyńska, M., Zapotoczny, S., 2013. J. Phys. Chem. C 117, 1136–1145. https://doi.org/10.1021/jp307832p.

Jachimska, B., Pajor, A., 2012. Bioelectrochemistry 87, 138–146. https://doi.org/10.1016/j.bioelechem.2011.09.004.

Jachimska, B., Tokarczyk, K., 2016. J. Phys. Chem. C 120. https://doi.org/10.1021/acs.jpcc.6b05020, 19678–19685.

Janik, M.E., Hoja-Lukowicz, D., Przybylo, M., 2016. In: Blumenberg, M. (Ed.), Human Skin Cancer, Potential Biomarkers and Therapeutic Targets. InTech. https://doi.org/10.5772/64666.

Jerabek-Willemsen, M., André, T., Wanner, R., Roth, H.M., Duhr, S., Baaske, P., Breitsprecher, D., 2014. J. Mol. Struct. 1077, 101–113. https://doi.org/10.1016/j.molstruc.2014.03.009.

Kılıç, A., Kok, F.N., 2018. Biointerphases 13, 011001. https://doi.org/10.1116/1.5000752.

Kobiela, T., Lelen-Kaminska, K., Stepulak, M., Lekka, M., Malejczyk, M., Arct, J., Majewski, S., 2013. Skin Res. Technol. 19, e200–e208. https://doi.org/10.1111/j.1600-0846.2012.00628.x.

Komorek, P., Martin, E., Jachimska, B., 2021. J. Mol. Sci. 22, 1322. https://doi.org/10.3390/ijms22031322.

Komorek, P., Wałek, M., Jachimska, B., 2020. Bioelectrochemistry 135, 107582. https://doi.org/10.1016/j.bioelechem.2020.107582.

Kycler, W., Grodecka-Gazdecka, S., Bręborowicz, J., Filas, V., Teresiak, M., 2006. Rep. Practical Oncol. Radiother. 11, 39–48. https://doi.org/10.1016/S1507-1367(06)71048-3.

Laidler, P., Gil, D., Pituch-Noworolska, A., Ciołczyk, D., Ksiazek, D., Przybyło, M., Lityńska, A., 2000. Acta Biochim. Pol. 47, 1159–1170.

Laidler, P., Lityńska, A., Hoja-Łukowicz, D., Łabędz, M., Przybyło, M., Ciołczyk-Wierzbicka, D., Pocheć, E., Trębacz, E., Kremser, E., 2006. Cancer Immunol. Immunother. 55, 112–118. https://doi.org/10.1007/s00262-005-0019-4.

Lekka, M., Laidler, P., Gil, D., Lekki, J., Stachura, Z., Hrynkiewicz, A.Z., 1999. Eur. Biophys. J. 28, 312–316. https://doi.org/10.1007/s002490050213.

Lekka, M., Pogoda, K., Gostek, J., Klymenko, O., Prauzner-Bechcicki, S., Wiltowska-Zuber, J., Jaczewska, J., Lekki, J., Stachura, Z., 2012. Micron 43, 1259–1266. https://doi.org/10.1016/j.micron.2012.01.019.

Li, X., Pei, Y., Zhang, R., Shuai, Q., Wang, F., Aastrup, T., Pei, Z., 2013. Chem. Commun. 49, 9908. https://doi.org/10.1039/c3cc45006f.

Lideikaitė, A., Mozūraitienė, J., Letautienė, S., 2017. actamedica 24. https://doi.org/10.6001/actamedica.v24i1.3460.

Lityńska, A., Przybylo, M., Pocheć, E., Hoja-Łukowicz, D., Ciołczyk, D., Laidler, P., Gil, D., 2001. Melanoma Res. 11, 205–212. https://doi.org/10.1097/00008390-200106000-00001.

Magnez, R., Thiroux, B., Taront, S., Segaoula, Z., Quesnel, B., Thuru, X., 2017. Sci. Rep. 7, 17623. https://doi.org/10.1038/s41598-017-17963-1.

Marczyńska, D., Przybyło, M., 2013. Kosmos 62, 491–499.

Mayer, J.E., Swetter, S.M., Fu, T., Geller, A.C., 2014. J. Am. Acad. Dermatol. 71, 599.e1–599.e12. https://doi.org/10.1016/j.jaad.2014.05.046.

Mori, T., Ohtsuka, T., Okahata, Y., 2010. Langmuir 26, 14118–14125. https://doi.org/10.1021/la102260k.

Nowacki, L., Follet, J., Vayssade, M., Vigneron, P., Rotellini, L., Cambay, F., Egles, C., Rossi, C., 2015. Biosens. Bioelectron. 64, 469–476. https://doi.org/10.1016/j.bios.2014.09.065.

Ochwat, D., Hoja-Łukowicz, D., Lityńska, A., 2004. Melanoma Res. 14, 479–485. https://doi.org/10.1097/00008390-200412000-00007.

Peiris, D., Markiv, A., Curley, G.P., Dwek, M.V., 2012. Biosens. Bioelectron. 35, 160–166. https://doi.org/10.1016/j.bios.2012.02.037.

Peiris, D., Spector, A.F., Lomax-Browne, H., Azimi, T., Ramesh, B., Loizidou, M., Welch, H., Dwek, M.V., 2017. Sci. Rep. 7, 43006. https://doi.org/10.1038/srep43006.

Piñero-Madrona, A., Goméz-Ruiz, A.J., Ruiz-Merino, G., Martínez-Barba, E., Cerezuela-Fuentes, P., Rodríguez-López, J.N., Cabezas-Herrera, J., 2019. J. Am. Acad. Dermatol. 80, 806–808. https://doi.org/10.1016/j.jaad.2018.09.034.

Pocheć, E., Lityńska, A., Amoresano, A., Casbarra, A., 2003. Biochim. Biophys. Acta Mol. Cell Res. 1643, 113–123. https://doi.org/10.1016/j.bbamcr.2003.10.004.

Prieto, V.G., Shea, C.R., 2016. In: Torres-Cabala, C.A., Curry, J.L. (Eds.), Genetics of Melanoma. Springer New York, New York, NY, pp. 85–113. https://doi.org/10.1007/978-1-4939-3554-3_4.

Przybyło, M., Hoja-Lukowicz, D., Lityńska, A., Laidler, P., 2002. Cancer Cell Int. 2, 6. https://doi.org/10.1186/1475-2867-2-6.

Re, S., Nishima, W., Miyashita, N., Sugita, Y., 2012. Biophys. Rev. 4, 179–187. https://doi.org/10.1007/s12551-012-0090-y.
Sandoval-Altamirano, C., Sanchez, S.A., Ferreyra, N.F., Gunther, G., 2017. Colloids Surf. B Biointerfaces 158, 539–546. https://doi.org/10.1016/j.colsurfb.2017.07.026.
Senkara-Barwijuk, E., Kobiela, T., Lebed, K., Lekka, M., 2012. Biosens. Bioelectron. 36, 103–109. https://doi.org/10.1016/j.bios.2012.04.014.
Sobiepanek, A., Baran, J., Milner-Krawczyk, M., Kobiela, T., 2020a. Open access. J. Biomed. Sci. 2 (1), 275–278. https://doi.org/10.38125/OAJBS.000161.
Sobiepanek, A., Kobiela, T., 2018. Rev. Res. Cancer Treat. 4, 4–12.
Sobiepanek, A., Kobiela, T., 2022. In: Ossandon, M., Baker, H., Rasooly, A. (Eds.), Biomedical Engineering Technologies, Methods in Molecular Biology, 2393. Humana, New York, NY. https://doi.org/10.1007/978-1-0716-1803-5_28.
Sobiepanek, A., Kowalska, P.D., Soszyńska, M., Kobiela, T., Ścieżyńska, A., 2020b. Rev. Res. Cancer Treat. 6, 67–78.
Sobiepanek, A., Milner-Krawczyk, M., Bobecka-Wesołowska, K., Kobiela, T., 2016. J. Photochem. Photobiol. B Biol. 164, 264–270. https://doi.org/10.1016/j.jphotobiol.2016.09.038.
Sobiepanek, A., Milner-Krawczyk, M., Lekka, M., Kobiela, T., 2017. Biosens. Bioelectron. 93, 274–281. https://doi.org/10.1016/j.bios.2016.08.088.
Sobiepanek, A., Paone, A., Cutruzzolà, F., Kobiela, T., 2021. Eur. Biophys. J. 50, 523–542. https://doi.org/10.1007/s00249-021-01514-8.
Ścieżyńska, A., Sobiepanek, A., Kowalska, P.D., Soszyńska, M., Łuszczyński, K., Grzywa, T.M., Krześniak, N., Góźdź, A., Włodarski, P.K., Galus, R., Kobiela, T., Malejczyk, J., 2021. Cancers 13, 6244. https://doi.org/10.3390/cancers13246244.
Staniszewska, M., Sobiepanek, A., Małgorzata, G., Peña-Cabrera, E., Arroyo-Córdoba, I. J., Michalina, K., Kuryk, Ł., Wieczorek, M., Koronkiewicz, M., Kobiela, T., Ochal, Z., 2020. Eur. J. Med. Chem. 191, 112139 https://doi.org/10.1016/j.ejmech.2020.112139.
Sung, H., Ferlay, J., Siegel, R.L., Laversanne, M., Soerjomataram, I., Jemal, A., Bray, F., 2021. CA A Cancer J. Clin. 71, 209–249. https://doi.org/10.3322/caac.21660.
Suutari, T., Rahman, S.N., Vischer, H.F., van Iperen, D., Merivaara, A., Yliperttula, M., Leurs, R., Kool, J., Viitala, T., 2020. Anal. Chem. 92, 14509–14516. https://doi.org/10.1021/acs.analchem.0c02652.
Viitala, T., Granqvist, N., Hallila, S., Raviña, M., Yliperttula, M., 2013. PLoS One 8, e72192. https://doi.org/10.1371/journal.pone.0072192.
Wang, W., Yang, Y., Wang, S., Nagaraj, V.J., Liu, Q., Wu, J., Tao, N., 2012. Nat. Chem. 4, 846–853. https://doi.org/10.1038/nchem.1434.
Weder, G., Hendriks-Balk, M.C., Smajda, R., Rimoldi, D., Liley, M., Heinzelmann, H., Meister, A., Mariotti, A., 2014. Nanomed. Nanotechnol. Biol. Med. 10, 141–148. https://doi.org/10.1016/j.nano.2013.07.007.
Yanase, Y., Hiragun, T., Ishii, K., Kawaguchi, T., Yanase, T., Kawai, M., Sakamoto, K., Hide, M., 2014. Sensors 14, 4948–4959. https://doi.org/10.3390/s140304948.
Zhou, S., Dong, X., Veillon, L., Huang, Y., Mechref, Y., 2017. Anal. Bioanal. Chem. 409, 453–466. https://doi.org/10.1007/s00216-016-9996-8.
Zhou, T., Marx, K.A., Dewilde, A.H., McIntosh, D., Braunhut, S.J., 2012. Anal. Biochem. 421, 164–171. https://doi.org/10.1016/j.ab.2011.10.052.